Research Square

Preprints are preliminary reports that have not undergone peer review.
They should not be considered conclusive, used to inform clinical practice,
or referenced by the media as validated information.

Cytoprotective and antifibrotic effects of losartan on human orbital adipose-derived mesenchymal stem cells (hOA-MSCs) in an in vitro oxidative stress model

Sevınj Eyubova
Eskişehir Osmangazi University
Burcugul Altug
Eskişehir Osmangazi University
Merve Nur Soykan
Eskişehir Osmangazi University
Didem Akincilar
Eskişehir Osmangazi University
Fatih Apaydın
Eskişehir Osmangazi University
Onur Ozalp
Eskişehir Osmangazi University
Eray Atalay
eatalay@ogu.edu.tr

Eskişehir Osmangazi University

Research Article

Keywords: mesenchymal stem cell, losartan, oxidative stress, cytoprotection, fibrosis

Posted Date: September 1st, 2026

DOI: https://doi.org/10.21203/rs.3.rs-10729812/v1

License: This work is licensed under a Creative Commons Attribution 4.0 International License.
Read Full License

Additional Declarations: No competing interests reported.

Abstract

Background

We investigated the effects of Losartan (LST) on cell viability, reactive oxygen species (ROS) production, and fibrosis-related gene expression in an *in vitro* oxidative stress model using human orbital adipose tissue-derived mesenchymal stem cells (hOA-MSCs).

Methods

hOA-MSCs were isolated from blepharoplasty surgical waste tissue and characterized. Non-cytotoxic LST concentrations and the optimal H_2O_2 concentration (25μM) for oxidative stress induction were determined. Under oxidative stress, hOA-MSC proliferation was assessed via MTT assay, ROS production was analyzed by flow cytometry, and TGFβ1 secretion was measured by ELISA. Fibrosis-, angiogenesis-, and survival-related gene expressions were evaluated using qPCR at 72 hours.

Results

Losartan significantly increased hOA-MSC proliferation and reduced ROS levels at 2 nM, 10 nM, and 50 nM concentrations at 72 hours under oxidative stress. Gene expression analyses showed concentration-dependent modulations, *VEGF* was upregulated at 10 nM, whereas *LOX* expression was suppressed at 10 nM and 50 nM. *PRKG1* expression was suppressed across all treated groups. Furthermore, *SIRT1* and *TGFβR1* expression levels increased across all LST concentrations. AT_2R expression was upregulated at 10 nM and 50 nM, while strong upregulations of *TGFβ1* and *TGFβ3* expressions were observed particularly at 10 nM and 50 nM.

Conclusion

Losartan exerted distinct concentration- and time-dependent cytoprotective and antifibrotic effects on hOA-MSCs under oxidative stress. The drug enhanced proliferation, cleared ROS, suppressed *LOX*, and shifted the balance toward protective pathways (*SIRT1*, AT_2R, and *TGFβ3*). These molecular mechanisms support the potential therapeutic application of Losartan against ocular surface and periocular tissue fibrosis.

CLINICAL TRIAL REGISTRATION

Not applicable

INTRODUCTION

Following ocular surface injury—whether from infection, mechanical trauma, or refractive surgery—dysregulated wound healing can culminate in fibrosis and permanent loss of corneal transparency. Crucially, recent evidence highlights that oxidative stress, driven by the excessive accumulation of reactive oxygen species (ROS), serves as a fundamental upstream orchestrator of this fibrotic cascade [1]. Tissue injury triggers an immediate surge in intracellular ROS—such as superoxide (O_2^-), hydrogen peroxide (H_2O_2), and hydroxyl radicals (-OH)—which overwhelms the endogenous antioxidant defense mechanisms. This state of oxidative stress not only causes direct cellular damage but also functions as a potent signaling trigger that upregulates and sustains the transforming growth factor-beta (TGF-β) pathway, the master regulator of myofibroblast differentiation and tissue fibrosis. Therefore, targeting and mitigating post-injury oxidative stress represents a vital therapeutic checkpoint to prevent the initiation and progression of corneal scar formation [2, 3].

Losartan (LST), a selective angiotensin II type 1 (AT_1) receptor antagonist traditionally used to treat systemic cardiovascular and renal diseases [4], has recently emerged as a promising candidate for anti-scarring therapies. Beyond its canonical hemodynamic actions, contemporary studies indicate that LST possesses significant cytoprotective and anti-oxidative properties. At the molecular level, LST-mediated AT_1 receptor blockade has been shown to alleviate ROS generation, restore mitochondrial membrane potential, and rescue cells from oxidative damage. Concurrently, LST facilitates the upregulation of cytoplasmic sirtuin 1 (SIRT1)—a crucial NAD^+-dependent deacetylase that maintains cell survival by clearing ROS—and shifts angiotensin II signaling toward the angiotensin II type 2 (AT_2) receptor/cyclic guanosine monophosphate (cGMP) axis, which directly suppresses profibrotic genes and ECM overproduction [5, 6, 7, 8]. While LST's capacity to reduce corneal opacity has been noted *in vivo* animal models [9, 10, 11, 12, 13, 14], the precise molecular mechanisms regarding how LST modulates downstream fibrotic genes specifically in response to an oxidative stress challenge remain to be fully characterized.

To address this gap, we investigated the therapeutic and cytoprotective capacity of LST in a periocular-derived *in vitro* oxidative stress model. Human orbital adipose tissue-derived mesenchymal stem cells (hOA-MSCs) were used as the cell source, given their proven potential to differentiate into ocular-lineage cells, including corneal epithelial-like cells and functional keratocytes under specific microenvironmental cues [15, 16, 17]. The primary objective of this work is to elucidate how varying concentrations of LST influence cell viability, execute ROS scavenging activity, and modulate the gene expression profiles of key fibrosis-, angiogenesis-, and survival-associated targets (*TGFβR1, PRKG1, SIRT1, AT_2R, LOX, VEGF, TGFβ1*, and *TGFβ3*) directly under H_2O_2-induced oxidative stress. Understanding how LST modulates these pathways may help explain its reported benefit in reducing corneal scarring and point to its potential as an anti-scarring treatment in ocular surface disease.

MATERIAL AND METHODS

2.1 Isolation and culture of hOA-MSCs

The orbital adipose tissue, which is waste tissue after blepharoplasty surgery, was obtained from the Ophthalmology Clinics of Eskişehir Osmangazi University Hospital. (IRB approval ESOGU Non-Interventional Clinical Research Ethics Committee no: 30:13.05.2020). hOA-MSCs cells were isolated using the explant culture method. Initially, the tissue was washed with Hank's Balanced Salt Solution (HBSS, Capricorn Scientific, Ebsdorfergrund, Germany) containing 10% penicillin/streptomycin (Pen/St) and cut into 1 mm^3 pieces, which were then placed on the bottom of a 6-well culture plate and incubated in a laminar flow cabinet for 15 minutes to allow them to adhere. Subsequently, the tissue was cultured in medium containing 10% fetal bovine serum (FBS, Capricorn Scientific), 1% primosin (Invivogen, California, USA), 1% stable glutamine (Capricorn Scientific), and NutriStem XF Media supplement (Sartorius, Goettingen, Germany) NutriStem XF Media (Sartorius, Goettingen, Germany) was added to the medium, and the cells were cultured in a 37°C incubator (Panasonic, MCO-170M-PE, Kadoma, Japan) at 5% CO_2, 5% O_2, and 95% relative humidity.

2.1.1 Characterization of hOA-MSCs

At passage 3, immunophenotypic and *in vitro* trilineage differentiation characterization analyses of cultured hOA-MSCs were performed in accordance with the minimal criteria set out in the International Society for Stem Cell Research (ISSCR) guidelines.

2.1.2 Immunophenotypical characterization of hOA-MSCs by flow cytometry

Isolated hOA-MSCs were labeled with MSC surface marker antibodies at passage 3 to examine their stemness. CD73-, CD90-, CD105-, CD44-, CD29-, CD69-, CD34-, CD45-, CD25-, CD19-, HLA-DR-, and CD14-conjugated antibodies (BioLegend, San Diego, USA) were used for hOA-MSCs characterization. Briefly, the cell pellet was resuspended in 100 µL of binding solution, and 2 µL of each corresponding antibody was added to the suspension. The samples were incubated for 30 minutes at room temperature in the dark. After incubation, unbound antibodies were removed by centrifugation, and the cell pellet was resuspended in 300 µL of PBS. Flow cytometric analysis was then performed using a Novocyte 3500 (Agilent), and data were acquired and processed with NovoExpress 6.0 software (Agilent, CA, USA).

2.1.3 *In vitro* trilineage differentiation of hOA-MSCs for characterization

Differentiation assays were performed to demonstrate the capacity of the isolated hOA-MSCs to differentiate into adipogenic and osteogenic lineages in accordance with the guidelines of the International Society for Stem Cell Research (ISSCR).

Adipogenic differentiation

hOA-MSCs were seeded at a density of 1.5×10^5 cells per well in a 6-well culture plate. When the cells reached 80–90% confluence, adipogenic differentiation was induced by culturing in differentiation

medium for two weeks. The medium consisted of DMEM High Glucose (Capricorn Scientific, Ebsdorfergrund, Germany) supplemented with 10% FBS, 0.5 mM isobutyl-methylxanthine (IBMX), 5×10^{-7} M dexamethasone, 10 µg/mL insulin, 200 µM indomethacin, 1% penicillin–streptomycin, and 1% GlutaMAX. After the differentiation period, intracellular lipid accumulation was assessed by Oil Red O and adiponectin staining.

Osteogenic differentiation

hOA-MSCs were seeded at a density of 1.5×10^5 cells per well in a 6-well culture plate. When the cells reached 80–90% confluence, osteogenic differentiation was induced by culturing in DMEM High Glucose (Capricorn Scientific, Ebsdorfergrund, Germany) supplemented with 10% FBS, 100 nM dexamethasone, 0.05 µM ascorbate-2-phosphate, 10 mM β-glycerophosphate, 1% penicillin–streptomycin, and 1% GlutaMAX for four weeks. Following the differentiation period, calcium deposition was assessed by Alizarin Red S and osteonectin staining.

2.2 Establishment of an *in vitro* oxidative stress model

2.2.1. Determination of hydrogen peroxide (H_2O_2) concentration to establish an oxidative stress model in hOA-MSCs

To establish an *in vitro* oxidative stress model using hOA-MSCs, the non-cytotoxic concentration of hydrogen peroxide (H_2O_2) was determined by a cell viability/proliferation assay (MTT assay). hOA-MSCs were seeded in 96-well culture plates at a density of $3x10^3$ cells per well. After the cells adhered to the culture surface, the medium was removed and 100 µL of fresh medium containing H_2O_2 at concentrations of 10, 20, 30, 40, 50, 60, 70, 80, 90, and 100 µM were added per well. Twenty-four hours after exposure to H_2O_2, the non-cytotoxic concentration of H_2O_2 was determined by the MTT assay.

2.2.2. Determination of the effect of Losartan in an *in vitro* oxidative stress model

To determine the effect of LST in an *in vitro* oxidative stress model, hOA-MSCs were seeded in 96-well plates at a density of $5x10^3$ cells per well. After cell attachment, the medium was aspirated and, except for the control group, wells were treated with hydrogen peroxide (H_2O_2) at a final concentration of 25 µM and incubated for 24 hours. At the end of the incubation, the medium was removed, and 100 µL of fresh medium containing LST (MedChemExpress) at final concentrations of 0.1, 0.5, 1, 2, 5, 10, 20, 50, and 100 nM were added to the wells, excluding the control and positive-control wells. Following LST addition, plates were incubated for 24, 48, and 72 hours, after which the MTT assay was performed to assess the effects of LST.

2.3. Reactive oxygen species (ROS) test for determining oxidative stress

To determine the effect of LST on oxidative stress, ROS analysis was performed. hOA-MSCs, after removal of the old medium, were incubated with 1 mL of fresh medium containing 20 μM DCFH-DA (Cayman Chemical) per well for 60 minutes. At the end of incubation, wells were washed with DPBS (Capricorn Scientific) to remove the dye. Then, except for the control group, 1 mL of fresh medium containing 25 μM H_2O_2 was added to each well and incubated for 24 hours at 37°C. After incubation, the medium was aspirated, and wells were washed with DPBS to remove residual medium. Next, fresh medium containing the specified concentrations of LST (2 nM, 10 nM, 20 nM, and 50 nM) was added and incubated for 24, 48, and 72 hours. Thereafter, cells were detached with trypsin-EDTA and analyzed by flow cytometry on an Agilent NovoCyte 3500 flow cytometer. NovoExpress 6.0 software (Agilent, CA, USA) was used for data analysis.

2.4. TGFβ1 ELISA assay

An *in vitro* oxidative stress model was created in hOA-MSCs using H_2O_2, and after treatment with LST at concentrations of 2 nM, 10 nM, 20 nM, and 50 nM, TGF-β1 protein levels were measured in supernatants collected at 24, 48, and 72 hours using the Human TGF-β1 ELISA kit (SunRed Biotechnology Company, Shanghai, China) according to the manufacturer's protocol.

2.5. Gene expression analysis following LST application in an *in vitro* oxidative stress model

The *in vitro* oxidative stress model was established to examine changes in mRNA expression of fibrosis-associated *TGFβR1, SIRT1, PRKG1, AT_2R, LOX, VEGF, TGFβ1*, and *TGFβ3* as determined by quantitative real-time PCR (qPCR) using the Rotor-Gene system (QIAGEN, Hilden, Germany). Cells were exposed to predetermined LST concentrations of 2 nM, 10 nM, 20 nM, and 50 nM and incubated for 72 hours. Total RNA from LST-treated cells was isolated using the miRNeasy Micro Kit (QIAGEN) according to the manufacturer's protocol. The extracted RNA was reverse-transcribed into cDNA using the QuantiTect Reverse Transcription Kit (QIAGEN). Real-time PCR was performed on the cDNA using gene-specific primers (QIAGEN) and the QuantiNova SYBR Green PCR Kit (QIAGEN) with a Rotor-Gene instrument. Ct values were determined using GAPDH as the reference gene, and relative quantification was performed using the $2^{-\Delta\Delta Ct}$ method.

2.6 Statistical Analysis

Each experiment was conducted with at least three independent replicates, and data are presented as mean ± SEM. Statistical analyses were performed using SPSS 20.0 (or later versions). One-way ANOVA followed by Tukey's post-hoc test was applied for statistical comparisons. Significance levels were set at $*p < 0.05$, $**p < 0.01$, and $***p < 0.001$.

RESULTS

3.1 Isolation and Culture of Human Adipose Tissue-Derived Mesenchymal Stem Cells (hOA-MSCs)

Isolated hOA-MSCs were expanded and cultured up to the third passage. The cultured cells adhered sparsely to culture vessels and exhibited spindle-shaped and stellate fibroblast-like morphologies. The hOA-MSCs proliferated and formed colonies. The isolated and cultured cells reached confluence (70–80%) seven days after initial attachment was observed (Fig. 1A-C).

hOA-MSCs were differentiated along two distinct lineages. Adipogenic differentiation was associated with positive Oil Red O histological staining and adiponectin immunocytochemical staining. Osteogenic differentiation was associated with positive Alizarin Red S histological staining and osteocalcin immunocytochemical staining (Fig. 1D-I).

Up to the third passage, immunophenotypic analysis of cultured hOA-MSCs was performed using antibodies specific to surface antigens defined as the minimal immunophenotypic criteria by the International Society for Stem Cell Research (ISSCR) guidelines [21]. Positive expression was observed for CD73 (99.95%), CD90 (99.72%), CD105 (98.09%), CD44 (99.99%), and CD29 (99.92%), while CD69 (4.60%), CD34 (0.29%), CD45 (0.07%), CD25 (0.07%), CD19 (1.84%), HLA-DR (0.00%), and CD14 (4.74%) were negative (Fig. 2).

3.2 Determination of the effect of Losartan on the *in vitro* oxidative stress model

Across the analysis, the concentrations of LST used (0.1, 0.5, 1, 2, 5, 10, 20, 50, and 100 nM) did not induce cytotoxic effects, independently of concentration or exposure duration (Fig. 3A). To establish an oxidative stress model, the H_2O_2 concentration that produced approximately 80% viability after 24 hours was determined by linear regression to be 25 µM (Fig. 3B).

An oxidative stress model was established in hOA-MSCs using H_2O_2, and viability and proliferation analyses were performed to determine the proliferative concentration of LST. Cells were first exposed to 25 µM H_2O_2 for 24 hours, followed by exposure to LST and assessment by an MTT assay. Based on these results, although the oxidative stress model was established, LST at 2 nM, 10 nM, and 50 nM increased cell viability by approximately 120% relative to control at 72 hours. The therapeutic concentrations of LST against oxidative stress at 72 hours were determined to be 2 nM, 10 nM, 20 nM, and 50 nM (Fig. 3C).

3.3 Reactive Oxygen Species (ROS) Test for Oxidative Stress Assessment

An oxidative-stress model was established in hOA-MSCs by exposure to H_2O_2, after which LST was applied at concentrations of 2 nM, 10 nM, 20 nM, and 50 nM. Reactive oxygen species (ROS) activity was determined by flow cytometry.

At 24, 48, and 72 hours, the effects of LST concentrations on ROS production were evaluated. ROS production was lower than in the positive control (cells subjected to an H_2O_2-induced oxidative stress throughout the experiment but not treated with LST), while ROS levels were similar to those in the negative control group (cells not treated with LST or H_2O_2). At 24 and 72 hours, ROS levels with 2 nM LST were observed to be equivalent to those of the control group. These findings suggest that post-injury oxidative stress in hOA-MSCs could be mitigated by a 2 nM LST concentration by reducing ROS levels, potentially exerting an anti-fibrotic effect (Fig. 4A).

3.4 ELISA Analysis

The TGFβ1 protein analysis showed a 1.8-fold increase in the positive control group at 72 hours. The negative control group exhibited a 1.64-fold increase. In cells treated with the oxidative stress model, 2 nM LST resulted in a 3.66-fold increase compared to the control at 72 hours, 10 nM LST showed a 2.72-fold increase, 20 nM LST showed a 2.59-fold increase, and 50 nM LST resulted in a 2.07-fold increase (Fig. 4B).

3.5 Gene Expression Results

Gene expression analysis performed in cells exposed to oxidative stress revealed notable alterations across multiple targets. *LOX* expression increased under oxidative stress by 1.9-fold and 1.92-fold at 2 nM and 20 nM LST, respectively, whereas it decreased by 0.59-fold at 10 nM and by 0.35-fold at 50 nM (Fig. 5A). For *PRKG1*, expression was reduced by 0.16-fold in the positive control and by 0.3-fold in the negative control group. Under oxidative stress, LST treatment further suppressed *PRKG1* expression by 0.3-fold at 2 nM, 0.14-fold at 10 nM, 0.96-fold at 20 nM, and 0.13-fold at 50 nM (Fig. 5B). In the case of AT_2R, expression decreased by 0.54-fold in the positive control and by 0.71-fold in the negative control. LST treatment under oxidative stress resulted in a 0.61-fold reduction at 2 nM, a 2.81-fold increase at 10 nM, a 0.87-fold decrease at 20 nM, and a 1.12-fold increase at 50 nM (Fig. 5C). *TGFβR1* expression decreased by 0.8-fold in the positive control and by 0.9-fold in the negative control. Treatment with Losartan (LST) markedly increased expression levels by 2.15-fold at 2 nM, 2.12-fold at 10 nM, 1.84-fold at 20 nM, and 2.76-fold at 50 nM (Fig. 5D). *SIRT1* expression increased by 1.07-fold in the positive control and by 2.19-fold in the negative control. Following LST exposure under oxidative stress, *SIRT1* levels were elevated by 1.59-fold at 2 nM, 1.58-fold at 10 nM, 1.33-fold at 20 nM, and 1.45-fold at 50 nM (Fig. 5E). For *TGFβ1*, expression increased by 1.05-fold in the positive control and by 1.8-fold in the negative control. LST treatment under oxidative stress conditions led to a 0.95-fold reduction at 2 nM, followed by increases of 3.21-fold, 1.88-fold, and 2.8-fold at 10 nM, 20 nM, and 50 nM, respectively (Fig. 5F). Finally, *TGFβ3* expression decreased by 0.18-fold in the positive control and by 0.32-fold in the negative control group. Under oxidative stress, LST treatment resulted in a 0.12-fold reduction at 2 nM

and strong upregulation by 9.84-fold, 0.95-fold, and 12.78-fold at 10 nM, 20 nM, and 50 nM, respectively (Fig. 5G). *VEGF* expression showed a 0.83-fold and 0.61-fold reduction in the positive and negative controls, respectively. LST treatment under oxidative stress led to a 0.97-fold, 0.57-fold, and 0.98-fold decrease at 2 nM, 20 nM, and 50 nM, while a 1.41-fold increase was detected at 10 nM (Fig. 5H).

DISCUSSION

Losartan (LST) is an oral medication used to treat hypertension, diabetic nephropathy, heart failure, and left ventricular dilation [4]. Beyond its antihypertensive effects, LST has been shown to inhibit TGF-β–mediated pathways, thereby exerting antifibrotic properties [7]. In the present study, hOA-MSCs were treated with various concentrations of LST (0.1–100 nM) across multiple time points (24, 48, and 72 h). Notably, 2 nM, 10 nM, and 50 nM LST significantly enhanced cell proliferation after 72 hours of exposure. Under oxidative stress conditions, ROS levels were elevated at 24 and 72 hours but were normalized by 2 nM LST treatment, reaching values comparable to the unstressed control. These findings are consistent with prior evidence suggesting that LST mitigates ROS generation, and such reduction in oxidative stress may contribute to its antifibrotic effects given the established association between ROS accumulation and fibrogenesis [18].

Mesenchymal stem cells (MSCs) are widely used in regenerative medicine for the treatment of tissue damage resulting from various pathological conditions or trauma [19]. Human orbital adipose tissue constitutes a highly practical, clinically accessible, and minimally invasive autologous source of MSCs, routinely harvested as medical waste during common ophthalmic procedures such as blepharoplasty or levator resection [20]. Owing to their periocular anatomical origin and documented capacity to differentiate into ocular-lineage cells, hOA-MSCs offer a clinically accessible, periocular-derived *in vitro* platform to probe the molecular pathways through which LST acts under oxidative stress [15, 16, 17].

By day 7 of primary culture, hOA-MSCs adhered to culture dishes and displayed a spindle-shaped fibroblast-like morphology with stellate extensions. At passage 3, flow cytometric characterization confirmed that the cells highly expressed standard mesenchymal surface markers (CD44, CD90, CD105 and CD 29) while remaining negative for hematopoietic and endothelial markers (CD69, CD25, CD19, CD34, CD45, CD14, HLA-ABC, and HLA- DR) [21]. When induced with appropriate culture supplements, the hOA-MSCs differentiated toward adipogenic and osteogenic lineages. Thus, the isolated hOA-MSCs exhibited MSC characteristics consistent with the criteria defined by the International Society for Stem Cell Research (ISSCR) [21]. Intriguingly, while previous studies have reported cytotoxic effects of LST at concentrations around 20 nM in specific pulmonary and endometrial cancer cell lines [22, 23], no cytotoxicity was observed in hOA-MSCs within the evaluated dose range (0.1–100 nM). This absence of toxicity may be attributed to the intrinsic chemoresistance mechanisms typical of multipotent stem cells, often driven by active ATP-binding cassette (ABC) transporter-mediated drug efflux [24, 25].

Superoxide (O_2^-), hydrogen peroxide (H_2O_2), and hydroxyl radicals (·OH) are among the principal ROS that can disrupt cellular homeostasis by inhibiting the activity of various biomolecules [26]. Oxidative stress

caused by ROS accumulation leads to cellular damage and dysfunction, reducing the viability and immunomodulatory activity of MSCs [27]. In the present study, intracellular ROS levels were quantified using the ROS-sensitive fluorescent probe DCFH-DA, as previously described by Raei et al. [28]. Oxidative stress was experimentally induced in hOA-MSCs through H_2O_2 exposure, followed by treatment with LST at concentrations of 2, 10, 20, and 50 nM. Consistent with previous findings, LST reduced ROS production, reinforcing its cytoprotective role under oxidative stress [28].

Transforming growth factor beta-1 (TGFβ1) is an important cytokine secreted by many cell types in the body and is implicated in fibrosis development. Among the three TGF-β isoforms, TGFβ1 and TGFβ3 are widely expressed signaling proteins secreted by multiple cell types. TGFβ isoforms signal through two cell-surface receptors known as TGFβ type I and type II receptors (TβRI and TβRII) [29, 30]. Our gene and protein expression analyses revealed that oxidative stress significantly upregulated both *TGFβ1* and *TGFβR1* expressions. At the protein level, ELISA analysis confirmed an elevated secretion of TGFβ1 at 24 and 72 h post-stress, indicating the activation of a canonical profibrotic feedback loop. However, LST treatment introduced a distinct modulation: while *TGFβ1* and *TGFβR1* transcripts remained elevated under certain concentrations, *TGFβ3* expression exhibited an outstanding upregulation. Specifically, 10 nM LST induced a 9.84-fold increase under stress, while 50 nM LST generated a 12.78-fold increase. Given that *TGFβ3* possesses well-known anti-scarring properties that counteract the profibrotic actions of *TGFβ1*, the remarkable elevation of *TGFβ3/ TGFβ1* expression ratio strongly implies that LST activates an intrinsic antifibrotic regulatory pathway in hOA-MSCs.

This homeostatic shift is further supported by the transcript regulation of *LOX*, a copper-dependent enzyme critical for collagen cross-linking and structural ECM stabilization. While oxidative stress expectedly increased *LOX* transcripts, treatment with 10 nM and 50 nM LST substantially suppressed its expression to 0.59-fold and 0.35-fold of the control, respectively. Downregulation of *LOX* effectively prevents irregular collagen cross-linking, which represents a key therapeutic checkpoint in halting scar formation.

Interestingly, our data revealed an intriguing regulatory anomaly regarding VEGF and LOX [31, 32, 33]. In mesenchymal systems, bidirectional signaling networks typically couple LOX activation with VEGF upregulation to drive angiogenesis [31, 32, 33]. In our hOA-MSC model, *PDGFA* transcripts were undetectable under basal conditions; yet, *LOX* expression remained responsive to LST in a concentration-dependent manner. Furthermore, we observed an inverse relationship where LST treatment led to a downregulation of *LOX* concurrent with an upregulation of *VEGF* (at 10 nM LST). This uncoupling suggests that the canonical LOX-VEGF pathway may be bypassed or regulated post-transcriptionally in hOA-MSCs, potentially via specific microRNAs (miRNAs) or alternative cell-specific signaling cascades. To fully validate this mechanism, future investigations utilizing selective PDGFR agonists/antagonists, targeted siRNA-mediated *LOX* silencing, and high-throughput miRNA profiling are highly recommended.

The balance between angiotensin II receptors, AT_1R and AT_2R, dictates the downstream pathophysiological outcomes of the renin-angiotensin system [34]. While AT_1R drives profibrotic and

proliferative signaling, *AT_2R* activation generally promotes cellular differentiation, apoptosis, and vasodilatory effects [34]. Crucially, *AT_2R* signaling has been reported to counteract fibrotic progression in renal models via the cGMP secondary messenger pathway [35, 34]. In the present study, 10 nM LST treatment markedly upregulated *AT_2R* expression by 2.81-fold under oxidative stress, whereas the stressed positive control exhibited a significant decline in *AT_2R* transcription. Correspondingly, 20 nM LST treatment successfully restored *PRKG1* (cGMP-dependent protein kinase) expression near to basal control levels. These findings indicate that LST-mediated *AT_1R* blockade successfully shifts the equilibrium toward the *AT_2R/cGMP* axis, thereby reinforcing an operational antifibrotic response under oxidative stress [35].

This cytoprotective mechanism is further sustained by sirtuin 1 (SIRT1) regulation [36]. SIRT1 is a crucial metabolic sensor that protects tissues from oxidative injury and fibrotic degeneration by deacetylating key transcription factors [36]. Conversely, its deficiency prompts myofibroblast accumulation and accelerates organ fibrosis [37]. Our results demonstrated that while *SIRT1* expression showed a relative decrease at higher LST doses compared to the unstressed negative control, its transcript levels remained significantly elevated in LST-treated cells compared to the untreated stressed positive control. This relative preservation of SIRT1 supports the enhanced cell viability and proliferative capacity observed in the MTT assays.

Literature indicates that SIRT1 overexpression can directly repress *TGFβR1* transcription and deactivate P-Smad2/3 signaling via physical binding, thereby blocking TGFβ-induced fibrogenesis [38]. In our study, independent analysis of *TGFβR1* revealed its upregulation following LST treatment under stress conditions. While a direct downregulation of *TGFβR1* would be more intuitive for an antifibrotic agent, the concurrent over-activation of *SIRT1* across all LST concentrations suggests that the actual anti-scarring protection is predominantly driven by downstream SIRT1-mediated epigenetic silencing and Smad deacetylation rather than a direct block of receptor transcription [38, 39].

Nonetheless, several limitations of the present study must be acknowledged. First, although hOA-MSCs represent a biologically relevant periocular model with a documented capacity for ocular-lineage differentiation, they were evaluated in their multipotent undifferentiated state rather than being pre-differentiated into corneal epithelial cells or mature functional keratocytes. Consequently, the observed kinetics may partially reflect general stem cell stress responses rather than isolated corneal stromal dynamics. Second, the prominent transcriptional upregulation of *TGFβ1* and *TGFβR1* following LST treatment appears paradoxical to the canonical mechanisms of an *AT_1* receptor blocker. While we hypothesize this to be an acute compensatory cellular mechanism or a negative feedback loop tied to the concurrent *SIRT1* hyper-activation, the precise intracellular feedback network remains speculative. Lastly, with the exception of the TGFβ1 ELISA assay, our findings rely heavily on quantitative real-time PCR transcript profiles. Given that mRNA expression does not always correlate linearly with functional translational changes, further validation at the protein level via Western Blot—specifically evaluating

downstream Smad2/3 phosphorylation and mature LOX cross-linking enzyme activity—is required to definitively substantiate these molecular pathways.

Collectively, these results demonstrate that LST exerts a comprehensive, multi-layered antifibrotic and cytoprotective effect on hOA-MSCs subjected to oxidative stress. The synchronized reduction of ROS, downregulation of *LOX*, preservation of *SIRT1*, upregulation of the AT_2*/cGMP* axis, and the establishment of a highly favorable anti-scarring *TGFβ3/TGFβ1* ratio collectively define a potent molecular network through which LST mitigates fibrogenesis. Further mechanistic verification focusing on miRNA interventions and Smad phosphorylation kinetics will be valuable to fully validate these intersecting pathways.

CONCLUSION

This study aimed to elucidate the molecular pathways by which the antifibrotic effects of LST may operate on hOA-MSCs. To this end, the expression levels of fibrosis-related genes *LOX, PRKG1, TGFβR1*, and AT_2R, the angiogenesis-related gene *LOX*-associated *VEGF*, as well as *SIRT1*, which influences cell proliferation and antifibrotic pathways, were examined in stressed hOA-MSCs to assess the effect of LST on their expression. The findings indicate that the effects of LST on hOA-MSCs vary with concentration and time. LST increased the expression of *SIRT1,* AT_2R, and *PRKG1*, while downregulating *LOX* expression Interestingly, LOX and VEGF exhibited an inverse relationship compared with that reported in the literature. It is recommended that future studies investigate the potential role of miRNAs that regulate the LOX-VEGF interaction.

In conclusion, this *in vitro* study indicates that Losartan (LST) exerts antifibrotic effects in human orbital adipose–derived mesenchymal stem cells (hOA-MSCs) through the modulation of *LOX, PRKG1,* AT_2R, and *SIRT1* expression. These findings suggest that LST may inhibit ROS-associated fibrosis by regulating these key antifibrotic and cytoprotective pathways in hOA-MSCs. Ultimately, identifying which of these pathways drive the antifibrotic response could point to targets for more selective anti-scarring therapies, offering an alternative to the broad, systemic effects of a drug like losartan. Confirming such targets, however, will require the protein-level validation noted above.

Declarations

ETHICS APPROVAL

All procedures performed in studies involving human tissue were in accordance with the ethical standards of the national research committee and with the 1964 Helsinki declaration and its later amendments or comparable ethical standards. IRB approval ESOGU Non-Interventional Clinical Research Ethics Committee no: 30-13.05.2020.

CONSENT TO PARTICIPATE

Informed consent was obtained from all individual participants included in the study.

CONFLICT OF INTEREST STATEMENT

The authors declare that they have no competing interest.

FUNDING INFORMATION

The authors acknowledge the support from the Eskisehir Osmangazi University, Scientific Research Projects (ESOGU-BAP Grant ID: 2023–2874) and Health Institutes of Türkiye (TÜSEB Grant ID: A232085).

Author Contribution

S.E. performed the experiments and wrote the original draft of the manuscript. B.A. performed the experiments, developed the methodology, and wrote the original draft. M.N.S. performed the experiments, developed the methodology, and wrote the original draft. D.A. performed the experiments and wrote the original draft. F.A. reviewed and edited the manuscript. O.O. reviewed and edited the manuscript. E.A. wrote the original draft, reviewed and edited the manuscript, administered the project, and acquired funding. All authors reviewed and approved the final manuscript.

Data Availability

The datasets generated and/or analyzed during the current study are not publicly available but are available from the corresponding author upon reasonable request.

References

1. Cejka C, Cejkova J. Oxidative stress to the cornea, changes in corneal optical properties, and advances in treatment of corneal oxidative injuries. Oxidative Med Cell Longev. 2015;2015(1):591530.
2. Anitua E, de la Fuente M, Muruzabal F, Reparaz I, del Olmo-Aguado S, Merayo-Lloves J, Alkhraisat MH. (2026). PRGF eye drops mitigate oxidative stress and fibrosis in an *in vitro* glaucoma model: The role of platelet and plasma enrichment. Eur J Pharm Sci, 107531.
3. Chen X, Yan H, Chen Y, Li G, Bin Y, Zhou X. Moderate oxidative stress promotes epithelial–mesenchymal transition in the lens epithelial cells via the TGF-β/Smad and Wnt/β-catenin pathways. Mol Cell Biochem. 2021;476(3):1631–42.
4. Simpson KL, McClellan KJ. Losartan: a review of its use, with special focus on elderly patients. Drugs Aging. 2000;16:227–50.

5. Yang L, Bataller R, Dulyx J, Coffman TM, Ginès P, et al. Attenuated hepatic inflammation and fibrosis in angiotensin type 1a receptor deficient mice. J Hepatol. 2005;43:317–23.
6. Kim H, Baek CH, Lee RB, Chang JW, Yang WS, Lee SK. Anti-Fibrotic Effect of Losartan, an Angiotensin II Receptor Blocker, Is Mediated through Inhibition of ER Stress via Up-Regulation of SIRT1, Followed by Induction of HO-1 and Thioredoxin. Int J Mol Sci. 2017;18(2):305.
7. Michel MC, Foster C, Brunner HR, Liu L. A systematic comparison of the properties of clinically used angiotensin II type 1 receptor antagonists. Pharmacol Rev. 2013;65(2):809–48.
8. Li J, Qu X, Ricardo SD, Bertram JF, Nikolic-Paterson DJ. Resveratrol inhibits renal fibrosis in the obstructed kidney: potential role in deacetylation of Smad3. Am J Pathol. 2010;177(3):1065–71.
9. Yao HW, Zhu JP, Zhao MH, Lu Y. Losartan attenuates bleomycin-induced pulmonary fibrosis in rats. Respiration. 2006;73(2):236–42.
10. Gay-Jordi G, Guash E, Benito B, Brugada J, Nattel S, Mont L, Serrano-Mollar A. (2013). Losartan prevents heart fibrosis induced by long-term intensive exercise in an animal model. PLoS ONE, 8(2), e55427.
11. Yun HH, Park S, Chung MJ, Son JY, Park JM, Jung SJ, Yim JH, Kang KK, Byeon S, Baek SM, Lee SW, Lee AR, Kim TH, Park JK, Jeong KS. Effects of losartan and L-serine in a mouse liver fibrosis model. Life Sci. 2021;278:119578.
12. Zou J, Zhou X, Ma Y, Yu R. Losartan ameliorates renal interstitial fibrosis through metabolic pathway and Smurfs-TGF-β/Smad. Biomed Pharmacother. 2022;149:112931.
13. Wilson SE. Two-phase mechanism in the treatment of corneal stromal fibrosis with topical losartan. Exp Eye Res. 2024;242:109884.
14. Sampaio LP, Hilgert GS, Shiju TM, Murillo SE, Santhiago MR, Wilson SE. Topical losartan inhibits corneal scarring fibrosis and collagen type IV deposition after Descemet's membrane-endothelial excision in rabbits. Exp Eye Res. 2022;216:108940.
15. Kumar A, Xu Y, Yang E, Wang Y, Du Y. Fidelity of long-term cryopreserved adipose-derived stem cells for differentiation into cells of ocular and other lineages. Exp Eye Res. 2019;189:107860.
16. Sikora B, Skubis-Sikora A, Kimsa-Furdzik M, Ciszek W, Kostrzewski M, Stojko J, Mazurek U, Gola J. Adipose-derived stem cells undergo differentiation after co-culture with porcine limbal epithelial stem cells. Stem Cell Res. 2019;41:101609.
17. da Martins M, de Carvalho TM, da Silva Cunha JL, Gomes P, D. A., de Goes AM. Induction of corneal epithelial differentiation of induced pluripotent and orbital fat-derived stem cells seeded on decellularized human corneas. Stem Cell Reviews Rep. 2022;18(7):2522–34.
18. Anan HH, Zidan RA, Shaheen MA, Fattah A-E, E. A. Therapeutic efficacy of bone marrow derived mesenchymal stromal cells versus losartan on adriamycin-induced renal cortical injury in adult albino rats. Cytotherapy. 2016;18(8):970–84.
19. Orbay H, Tobita M, Mizuno H. (2012). Mesenchymal stem cells isolated from adipose and other tissues: basic biological properties and clinical applications. *Stem cells international*, *2012*, 461718.

20. Mailey B, Hosseini A, Baker J, Young A, Alfonso Z, Hicok K, Wallace AM, Cohen SR. (2014). Adipose-derived stem cells: methods for isolation and applications for clinical use. Stem Cells Tissue Repair: Methods Protocols, 161–81.
21. Dominici M, Le Blanc K, Mueller I, Slaper-Cortenbach I, Marini F, Krause D, Deans R, Keating A, Prockop D, Horwitz E. Minimal criteria for defining multipotent mesenchymal stromal cells. The International Society for Cellular Therapy position statement. Cytotherapy. 2006;8(4):315–7.
22. Choi CH, Park Y-A, Choi J-J, Song T, Song SY, Lee Y-Y, Lee J-W, Kim T-J, Kim B-G, Bae D-S. Angiotensin II type I receptor and miR-155 in endometrial cancers: synergistic antiproliferative effects of anti-miR-155 and losartan on endometrial cancer cells. Gynecol Oncol. 2012;126(1):124–31.
23. Ashry O, Schnecko A, Clauss WG, Fronius M. Evidence for expression and function of angiotensin II receptor type 1 in pulmonary epithelial cells. Respir Physiol Neurobiol. 2014;195:37–40.
24. Chen D-R, Lu D-Y, Lin H-Y, Yeh W-L. Mesenchymal stem cell-induced doxorubicin resistance in triple negative breast cancer. Biomed Res Int. 2014;2014(1):532161.
25. Begicevic R-R, Falasca M. ABC transporters in cancer stem cells: beyond chemoresistance. Int J Mol Sci. 2017;18(11):2362.
26. Day RM, Suzuki YJ. (2005). Cell proliferation, reactive oxygen and cellular glutathione. *Dose-response*, *3*(3), dose-response. 003.003. 010.
27. Denu RA, Hematti P. Effects of oxidative stress on mesenchymal stem cell biology. Oxidative Med Cell Longev. 2016;2016(1):2989076.
28. Raei M, Ahmadi M, Abrotan S, Razavi A, Hedayatizadeh-Omran A, Shamshirian A, Heydari K, Saeedi M, Alizadeh-Navaei R. Effect of Losartan on Cell Proliferation and Reactive Oxygen Species Scavenging in Gastric Cancer Cell Lines. Eurasian J Med Oncol. 2024;8(2):135–40.
29. Huang T, Schor SL, Hinck AP. Biological activity differences between TGF-β1 and TGF-β3 correlate with differences in the rigidity and arrangement of their component monomers. Biochemistry. 2014;53(36):5737–49.
30. Mihaylova Z, Tsikandelova R, Sanimirov P, Gateva N, Mitev V, Ishkitiev N. Role of PDGF-BB in proliferation, differentiation and maintaining stem cell properties of PDL cells *in vitro*. Arch Oral Biol. 2018;85:1–9.
31. Baker A-M, Bird D, Welti JC, Gourlaouen M, Lang G, Murray GI, Reynolds AR, Cox TR, Erler JT. Lysyl oxidase plays a critical role in endothelial cell stimulation to drive tumor angiogenesis. Cancer Res. 2013;73(2):583–94.
32. Barratt SL, Flower VA, Pauling JD, Millar AB. VEGF (vascular endothelial growth factor) and fibrotic lung disease. Int J Mol Sci. 2018;19(5):1269.
33. Nouet S, Nahmias C. Signal transduction from the angiotensin II AT2 receptor. Trends Endocrinol Metabolism. 2000;11(1):1–6.
34. Yamamoto-Nonaka K, Koike M, Asanuma K, Takagi M, Trejo JAO, Seki T, Hidaka T, Ichimura K, Sakai T, Tada N. Cathepsin D in podocytes is important in the pathogenesis of proteinuria and CKD. J Am

Soc Nephrol. 2016;27(9):2685–700.
35. Abramicheva PA, Plotnikov EY. Hormonal regulation of renal fibrosis. Life. 2022;12(5):737.
36. Li P, Liu Y, Qin X, Chen K, Wang R, Yuan L, Chen X, Hao C, Huang X. SIRT1 attenuates renal fibrosis by repressing HIF-2α. Cell Death Discovery. 2021;7(1):59.
37. Bulvik R, Breuer R, Dvir-Ginzberg M, Reich E, Berkman N, Wallach-Dayan SB. SIRT1 deficiency, specifically in fibroblasts, decreases apoptosis resistance and is associated with resolution of lung-fibrosis. Biomolecules. 2020;10(7):996.
38. Liu Z-H, Zhang Y, Wang X, Fan X-F, Zhang Y, Li X, Gong Y-s, Han L-P. SIRT1 activation attenuates cardiac fibrosis by endothelial-to-mesenchymal transition. Biomed Pharmacother. 2019;118:109227.
39. Meng X-m, Nikolic-Paterson DJ, Lan HY. TGF-β: the master regulator of fibrosis. Nat Rev Nephrol. 2016;12(6):325–38.

Figures

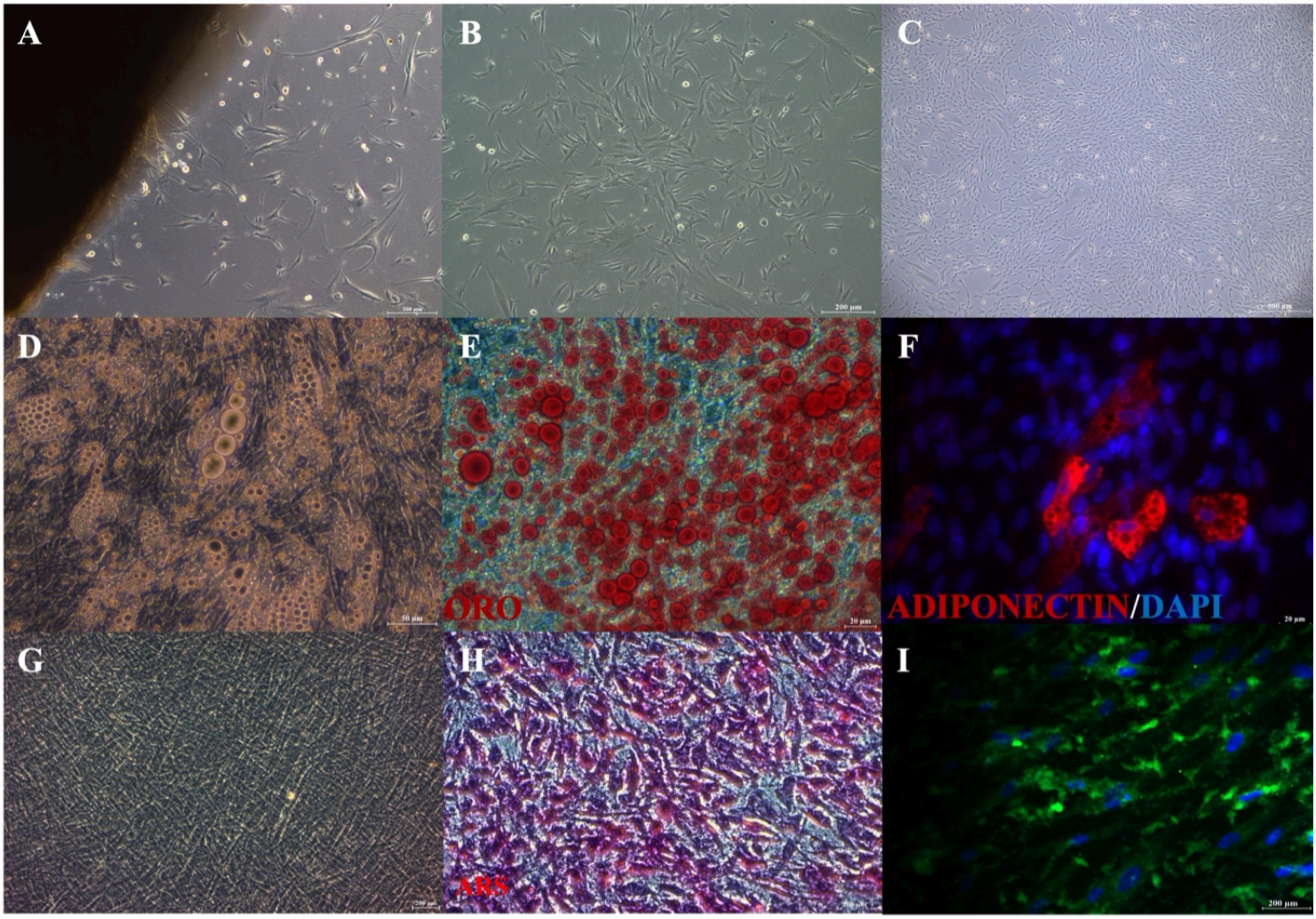


Figure 1

Isolation and characterization of hOA-MSCs. A) On day 7 of primary culture, cells migrating from the explant tissue were observed around the tissue fragment (Scale bar = 200 µm). B) At passage 1 (P1), hOA-MSCs obtained by the explant method predominantly displayed spindle-shaped and stellate fibroblast-like morphology. (Scale bars = 500 µm and 200 µm, respectively). C) A representative phase-contrast micrograph depicts the morphology of hOA-MSCs on day 3 of culture at passage 3 (P3) D) Phase-contrast inverted microscopic image of hOA-MSCs after 8 days of adipogenic induction, showing their morphological transition into adipocyte-like cells (Scale bar = 50 µm). E) Adipogenic differentiation was confirmed by the presence of neutral lipid vacuoles stained with Oil Red O (ORO) (Scale bar = 50 µm). F) Double immunofluorescence labeling with Adiponectin (red) and DAPI (blue) revealed lipid droplet accumulation under adipogenic induction (Scale bar = 20 µm). G) Osteogenic differentiation was demonstrated by the visualization of calcium-rich extracellular matrix deposits under phase-contrast microscopy (Scale bar = 200 µm). H) Mineral nodules were stained positively with Alizarin Red S staining (Scale bar = 200 µm). I) Osteogenic differentiation was demonstrated by immunofluorescence staining for osteocalcin (green) and DAPI (blue) (Scale bar = 200 µm).

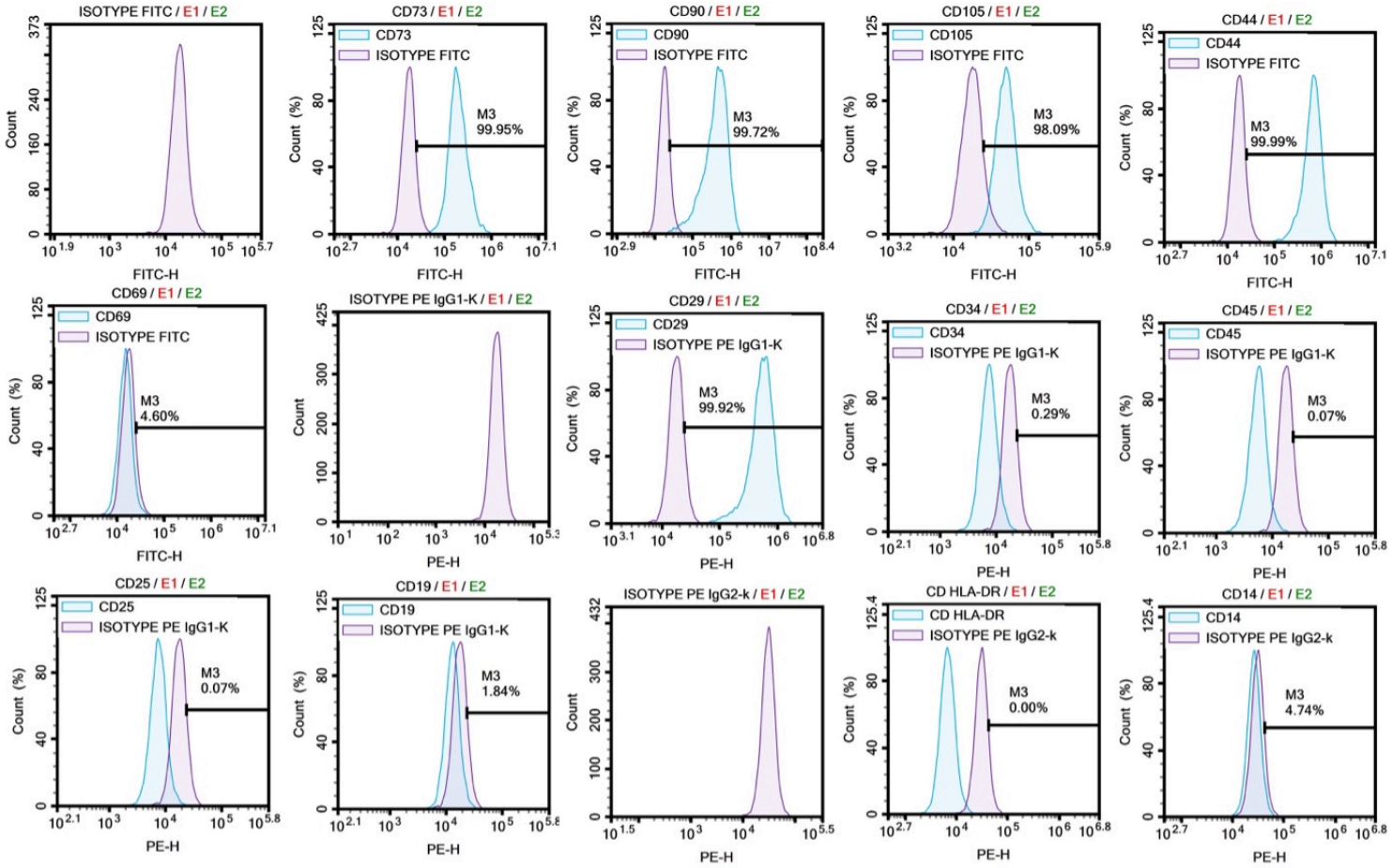


Figure 2

Immunophenotypic analysis of hOA-MSCs by flow cytometry in the third passage. CD73 (99.95%), CD90 (99.72%), CD105 (98.09%), CD44 (99.99%), and CD29 (99.92%) are positive while CD69 (4.60%), CD34 (0.29%), CD45 (0.07%), CD25 (0.07%), CD19 (1.84%), HLA-DR (0.00%), and CD14 (4.74%) are negative. On

the histogram, target antibodies are shown in blue and isotype antibodies (negative control) are shown in purple.

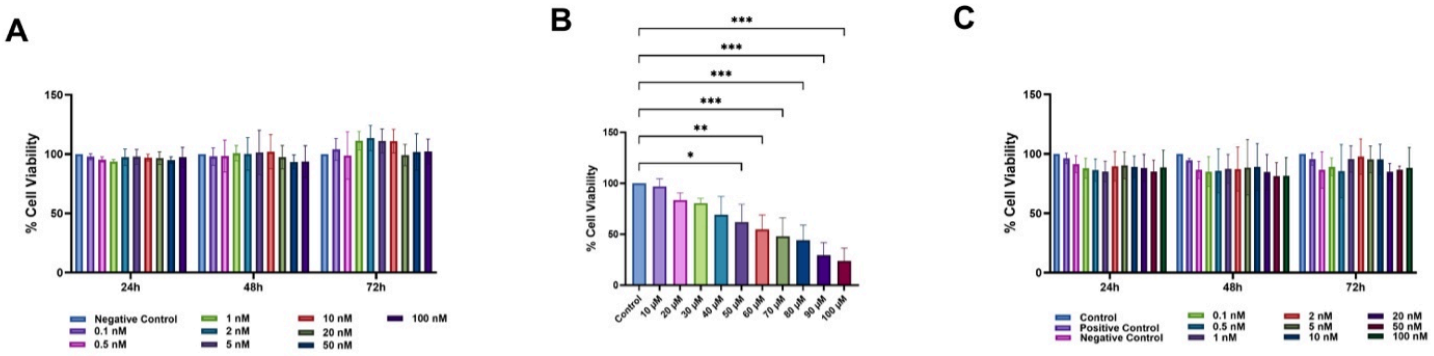


Figure 3

A) The cytotoxic effect of LST at concentrations of 0.1, 0.5, 1, 2, 5, 10, 20, 50, and 100 nM was determined by the MTT assay after 24, 48, and 72 hours of treatment. B) Cell viability analysis using MTT to establish an oxidative stress model with H_2O_2 concentrations of 10, 20, 30, 40, 50, 60, 70, 80, 90, and 100 µM. C) After establishing the oxidative stress model in hOA-MSCs, the therapeutic effect of LST was determined by cell viability analysis using MTT after exposure to concentrations of 0.1, 0.5, 1, 2, 5, 10, 20, 50, and 100 nM for 24, 48, and 72 hours (*p<0.05, **p<0.01, ***p<0.001).

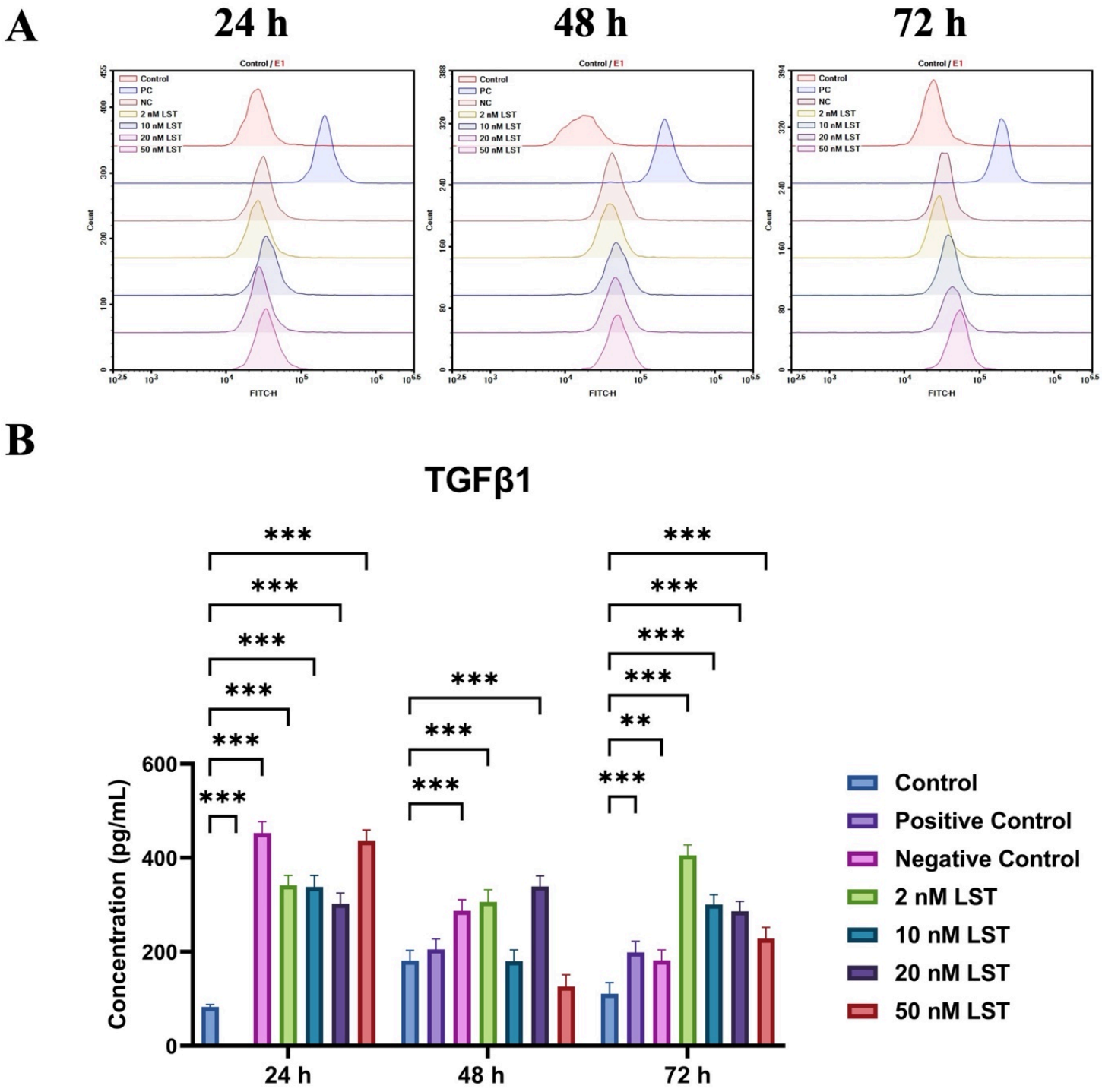


Figure 4

A) After establishing the oxidative stress model in hOA-MSC, the therapeutic effect of LST was determined by measuring the levels of reactive oxygen species (ROS) after exposure to concentrations of 2, 10, 20, and 50 nM of LST for 24, 48, and 72 hours (PC: Positive Control, NC: Negative Control). B) TGFβ1 protein analysis in samples obtained from the supernatants collected at 24, 48, and 72 hours after applying H_2O_2 and LST at concentrations of 2 nM, 10 nM, 20 nM, and 50 nM to hOA-MSC (*p<0.05, **p<0.01, ***p<0.001).

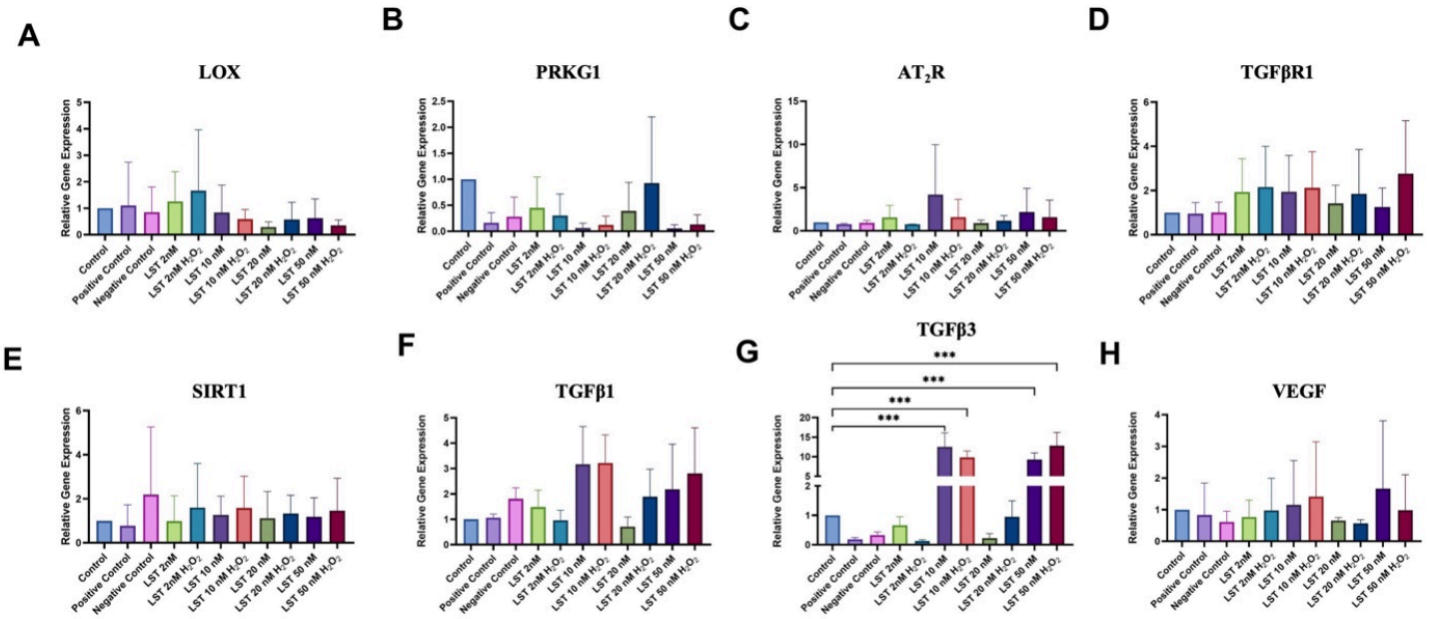


Figure 5

After establishing the oxidative stress model in hOA-MSC, the effect of LST was determined by analyzing the expression of A) *LOX*, B) *PRKG1*, C) *AT_2R*, D) *TGFβR1*, E) *SIRT1*, F) *TGFβ1*, G) *TGFβ3*, and H) *VEGF* genes after exposure to concentrations of 2 nM, 10 nM, 20 nM, and 50 nM for 72 hours (*p<0.05, **p<0.01, ***p<0.001).

Supplementary Files

This is a list of supplementary files associated with this preprint. Click to download.

- floatimage6.jpeg